Hindawi
Mathematical Problems in Engineering
Volume 2019, Article ID 7654543, 10 pages
https://doi.org/10.1155/2019/7654543

*Research Article*

# Research on Hydrodynamics with Water Temperature Characteristics and Spring Algal Blooms in a Typical Tributary Bay of Three Gorges Reservoir

**Yun Lang**[1,2], **LingLing Wang**[1,2], **Xin Cai**[3] and **Zijun Hu**[4]

[1] *State Key Laboratory of Hydrology-Water Resources and Hydraulic Engineering, Nanjing, China*
[2] *College of water Conservancy and Hydropower Engineering, Hohai University, Nanjing, China*
[3] *College of Mechanics and Materials, Hohai University, Nanjing, China*
[4] *Power China Huadong Engineering Corporation Limited, China*

Correspondence should be addressed to LingLing Wang; 706584934@qq.com

Received 4 April 2018; Revised 3 September 2018; Accepted 19 September 2018; Published 3 January 2019

Academic Editor: Ali Ramazani



After the impoundment of the Three Gorges Reservoir (TGR) in China, water environment problems induced by water temperature stratification in the Xiangxi Bay (XXB, a typical tributary bay of TGR) received wide attention. In this study, a 3-dimensional (3D) hydrodynamic and water temperature coupled model with the z-coordinate in the vertical direction was established with Delft3D software to simulate the continuous hydrodynamic and water temperature process of XXB in 2009, and the static stability and mixing depth were also analyzed. The results show that the upstream inflow is prevented from entering TGR with nutrients enriching and mixing in the upper and middle reach of XXB from winter to early spring, which is the primary cause of spring algal blooms in XXB. Therefore, measures such as improving the upstream hydrodynamic conditions and forcing the nutrients to flow into TGR in winter should be more effective in alleviating spring algal blooms than the artificial tide operation of TGR proposed by previous studies.

## 1. Introduction

Large-scale hydropower projects often cause environmental and ecological problems, such as harmful algal blooms [1, 2]. The completion of the Three Gorges Reservoir (TGR, China) on the Yangtze River in 2006 significantly elevated the water level and formed many reservoir bays in the upper tributaries. Xiangxi Bay (XXB), 32 km from the Three Gorges Dam, is the nearest and largest tributary bay in the upper reach of TGR, and spring algal blooms have been observed for many years [3, 4]. Long-term field monitoring concluded that specific water temperature stratification and hydrodynamic conditions were the important driving forces of spring algal blooms in the backwater region of TGR [5, 6]. Researchers suggested that a tide-type operation of TGR would be beneficial in reducing bloom frequencies in the tributary bays [7–9], but the operation was restricted by many factors such as flood control, water supply, and power supply of TGR. Moreover, transferring the hydrodynamic impact of the tide-type operation to the tributary bays of TGR is difficult, and therefore more operable measures are needed to alleviate spring algal blooms in the tributary bays.

To propose measures for spring algal blooms alleviation in XXB, a hydrodynamic-water temperature coupled numerical model was built to analyze the continuous hydrodynamic and water temperature process. Previous numerical studies of XXB were often based on vertical 2-dimensional (2D) [10] or 3-dimensional (3D) models with the $\sigma$-coordinate in the vertical direction [11, 12]. However, 2D models lack the ability to accurately simulate the secondary flow effects caused by the meandering reach of XXB. 3D models with the $\sigma$-coordinate would also cause large truncation error of the baroclinic pressure gradient force and the false water temperature stratification along the coordinate planes [13, 14]. Thus, a 3D model with the z-coordinate in the vertical

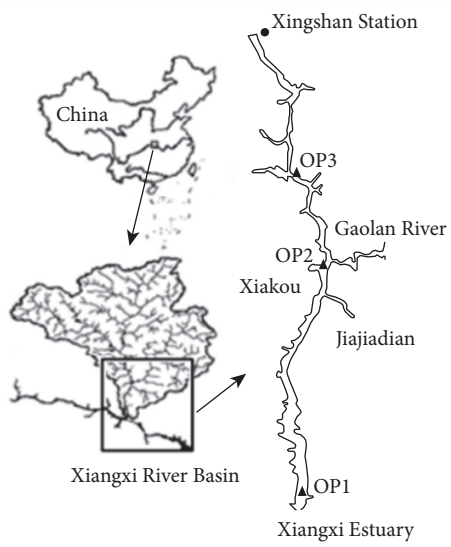


Figure 1: Location map of the Xiangxi River Basin and the modeled region of XXB.

direction was employed to improve the simulation accuracy in the present study.

Water temperature stratification stability is commonly evaluated by the vertical water temperature gradient [7], but this gradient cannot represent the stratification stability in the situation of different background water temperatures. Static stability, which is often employed to evaluate the density stratification stability of the sea [15] and atmosphere [16], can be used to overcome this drawback. The analysis of static stability and its vertical variation can promote understanding of hydrodynamics and water temperature characteristics in XXB.

Sverdrup [17] believed that mixing depth less than critical depth due to water temperature stratification was the primary cause of spring algal blooms in seas. The study of mixing depth can be used to explain the law of spring algal blooms and successions in XXB.

In the present study, a 3D hydrodynamic and water temperature coupled model of XXB was established with Delft3D software. Based on the analysis of water temperature distribution, hydrodynamic characteristics, static stability, and mixing depth, the formation process of spring algal blooms in XXB was deduced and effective measures to alleviate spring algal blooms were also proposed.

## 2. Materials and Methods

*2.1. Study Area.* The Xiangxi River (110°250′–111°060′E, 30°570′–31°340′N; Figure 1) is the nearest tributary in the upstream of the Three Gorges Dam (32 km), drains a 3095 $km^2$ watershed, and has a length of 94 km. After the initial water storage of TGR in June 2003, the Xiangxi River became a deep reservoir bay, and the backwater region extended to 40 km when the water level of TGR reached its designed level of 175 m. The peak discharge generally occurs from July to August and can reach 400 $m^3 \cdot s^{-1}$, while the rainfall in December to February is relatively less. The hydrologic characteristic in the Xiangxi River shows no obvious difference before and after the impoundment of TGR.

*2.2. Model Description and Application.* The Delft3D numerical model with the z-coordinate in the vertical direction is adopted to solve the incompressible shallow water equations, employing the Boussinesq assumption and approximation. The source and sink terms are used to represent the interlayer water exchange, specifically the quasi-3D approximation. The details of the governing equations and numerical methods can be found in the technical manual of the software [18]. The vertical water temperature distribution is simulated with the heat transfer conservation between incoming (solar shortwave and atmospheric long-wave radiation) and outgoing (convection, evaporation, and back radiation) sources. The heat exchange between water and river bed is assumed to be zero. The net heat increase in the study area is therefore equal to the increase of water temperature. The partial differential equations, in combination with an appropriate set of both initial and boundary conditions, are solved on finite difference orthogonal curved mesh. Since the maximum sediment concentration in XXB is only 0.8 $kg \cdot m^{-3}$, its effect on water density can be negligible. The UNESCO formulation [19] is chosen to construct for the equation of state:

$$\rho = 999.842594 + 6.793952 \cdot 10^{-2} T - 9.095290 \cdot 10^{-3} T^2 + 1.001685 \cdot 10^{-4} T^3 - 1.120083 \cdot 10^{-6} T^4 + 6.536332 \cdot 10^{-9} T^5, \quad (1)$$

where $\rho$ is water density ($kg \cdot m^{-3}$) and $T$ is water temperature (°C).

The number of grids in the horizontal direction is 25 × 192, with an average grid length of 100 m. The maximum number of layers in the vertical direction was 92, and the thicknesses of vertical layers is 0.5~2 m. The time step is set to 1 min according to the convergence criteria of Delft3D software.

*2.3. Definite Conditions.* The modeling period was from 1 January to 31 December in 2009. The initial conditions of hydrodynamics and water temperature were calculated by reiterating the process in January 1, 2009, until the temperature difference between the two periods was less than 0.1°C. The monthly averaged meteorological data for air temperature, relative humidity, sky cloudiness, and solar radiation were adopted. The upstream inflow boundary condition included the monitored discharge and water temperature distribution at Xingshan Station, and the water level and water temperature at Baqian Station were adopted as the boundary condition of the Xiangxi Estuary (Figure 2).

The important parameters calibrated in the XXB model included the bed roughness height ($Z_0$), drag coefficient ($C_d$), background horizontal and vertical eddy viscosity ($\nu_H^{back}$,

Table 1: Calibrated parameters in Delft3D for the XXB model.

| **Parameters** | $Z_0$ $(m)$ | $C_d$ (-) | $\nu_H^{back}$ ($m^2s^{-1}$) | $\nu_V^{back}$ ($m^2s^{-1}$) | $D_H^{back}$ ( $m^2s^{-1}$) | $D_V^{back}$ ($m^2s^{-1}$) |
|---|---|---|---|---|---|---|
| **Value used** | 0.15 | $1.255\times10^{-3}$ | 1.0 | $1.0\times10^{-5}$ | 0.1 | $1.0\times10^{-5}$ |

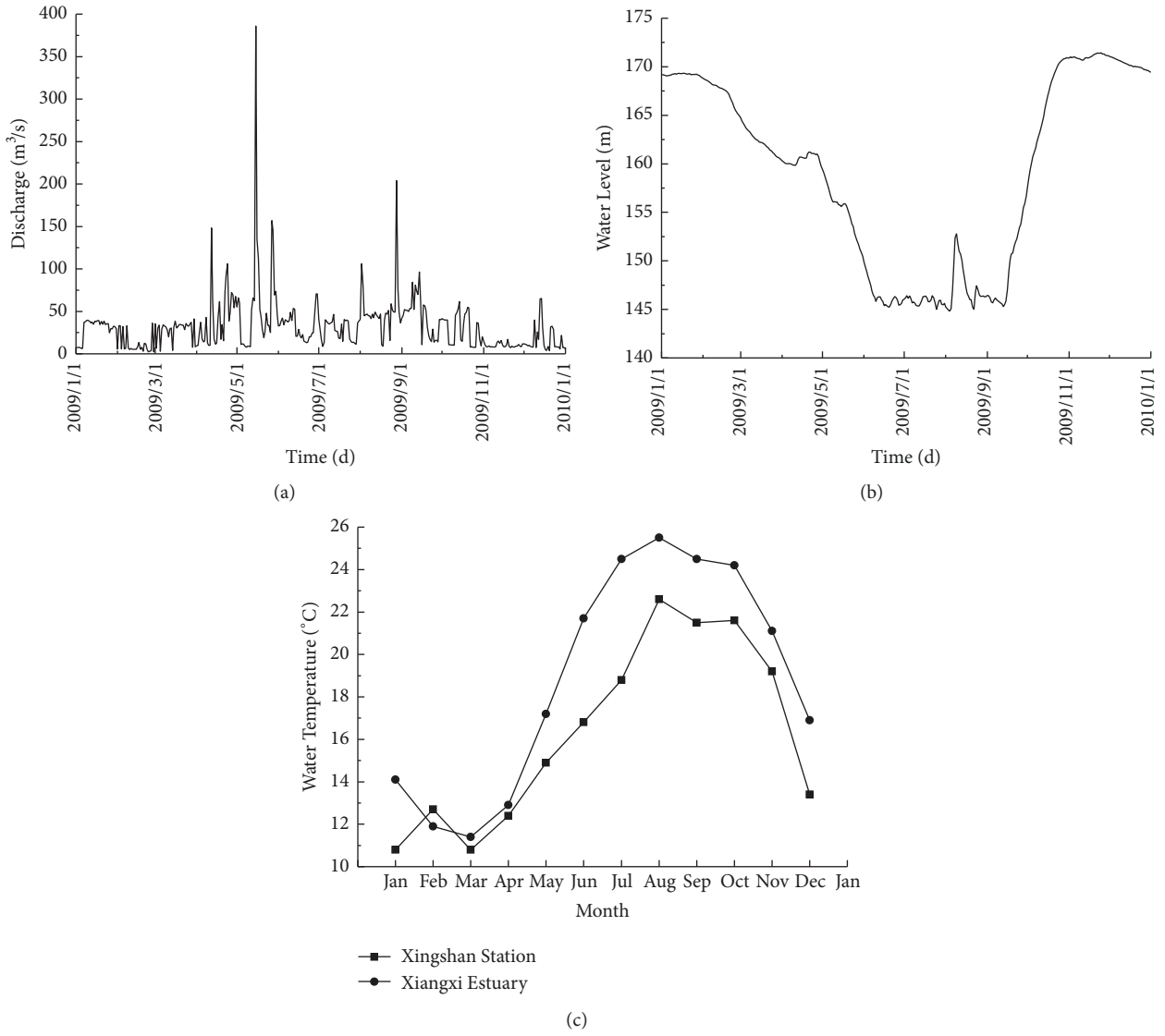


Figure 2: Model boundary conditions: (a) discharge at Xingshan Station; (b) water level of Xiangxi Estuary; (c) water temperature of Xingshan Station and Xiangxi Estuary.

$\nu_V^{back}$), and the background horizontal and vertical eddy diffusivity ($D_H^{back}$, $D_V^{back}$). In "Table 1", $Z_0$ and $C_d$ were calibrated with a trial and error method, and other parameters were determined according to the Delft3D manual.

*2.4. Model Calibration.* To evaluate the established hydrodynamic and water temperature coupled model, RMSE (Root Mean Square Error) is used to quantify the errors between the simulated data and the observed data.

The simulated water level is in close agreement with the observed value at Xingshan Station (Figure 3), and the RMSE value is 0.219. The water level fluctuation in different days has been accurately captured, indicating good performance of the present model in simulating the hydrodynamic process in the study area.

Three observation points (OP1 to OP3, Figure 1) which represent the downstream, midstream, and upstream of XXB, respectively, are selected to monitor the water temperature variation. "Figure 4" shows that the simulated vertical water temperature distribution of the 3 observation points is consistent with the observed data. The water temperature RMSE values of the 3 observation points in XXB are displayed in "Table 2". The RMSE value of OP3 is larger than that of the other observation points, possibly because OP1 and

Table 2: The RMSE values of water temperature of the 3 observation points in XXB.

| Observation points | Jan | Mar | May | Jul | Sep | Nov |
|---|---|---|---|---|---|---|
| **OP1** | 0.063 | 0.228 | 0.834 | 0.127 | 0.230 | 0.157 |
| **OP2** | 0.171 | 0.079 | 0.388 | 0.375 | 0.235 | 0.153 |
| **OP3** | 0.351 | 0.285 | 0.681 | 0.814 | 0.691 | 0.381 |

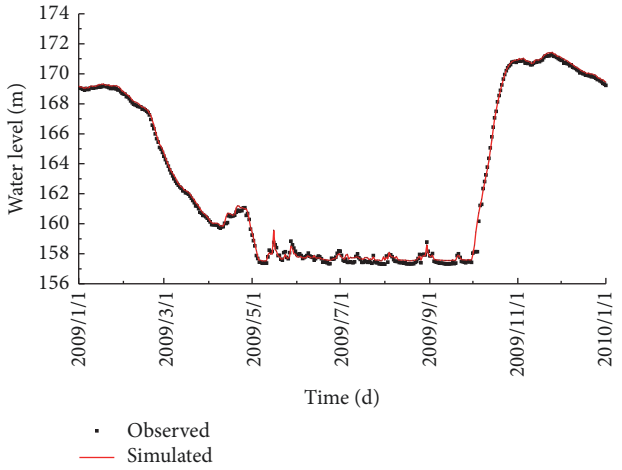


Figure 3: Observed and simulated water level at Xingshan Station in 2009.

OP2 are in the deep backwater region of TGR with higher hydrodynamic stability than OP3. In addition, the heat transport model used in the present model assumed that all of the solar radiation is absorbed by the surface layer and the bed heat transport is zero, which would cause water temperature error in the shallow water region larger than reported [20].

In general, the simulated results can be regarded as an acceptable approximation of the actual hydrodynamics and water temperature in the study area.

## 3. Results and Discussions

*3.1. Water Temperature Distribution.* According to the simulated results, the water temperature stratification in XXB can be divided into 3 typical periods: the uniform distribution period (from February to March), the strong stratification period (from April to September), and the bottom stratification period (from October to December and January). February, August, and December are selected to represent each typical period, respectively.

The thalweg water temperature profiles of the 3 typical months are shown in "Figure 5". In February, there is no thermocline because the water temperature of the upstream inflow is similar to that in TGR, with a maximum water temperature difference of only 1.1°C. In August, thermocline can be observed in both the surface and bottom regions since the summer solar radiation rapidly raises the surface water temperature while the internal heat transport is blocked by the thermoclines, and the maximum vertical water temperature gradient reaches 0.57°C·m$^{-1}$. TGR began to store water from September to November; then XXB was submerged in the backwater region. In December, the water temperature stratification occurred in the lower layer of the water (around 15 m above the river bed), since the temperature of the upstream inflow was lower than that in XXB.

*3.2. Hydrodynamic Characteristics.* The simulated velocity vector fields of the 3 typical months (Figure 6) show that the hydrodynamic characteristics in XXB are influenced by water temperature distribution.

In February, the water level of TGR was maintained at 168 m. The upstream discharge was 5 m$^3$·s$^{-1}$, and the water temperature was slightly higher than that of TGR. The water from TGR entered XXB from 65 m to 140 m in elevation at a flow velocity of 0.02~0.04 m·s$^{-1}$ while the upstream inflow was in the upper layer (Figure 6(a)). The velocity vectors suggest that the intrusion flow from TGR and the upstream inflow were encountered at a distance of 28 km from the estuary; then both of the flows reversed, forming two vertical vortexes in XXB. It can be inferred that there is strong vertical mixing in the upstream of XXB, inducing the transport of nutrients from the lower layer to the upper layer.

In August, the water level of TGR fluctuated from 146 to 153 m. The upstream discharge was 50 m$^3$·s$^{-1}$, and the water temperature was about 22.6°C (2°C lower than that of TGR). The intrusion flow from TGR to XXB was in the upper layer, while the upstream inflow was along the river bed (Figure 6(b)). Because of the strong water temperature stratification at the interface, the two flows in opposite directions did not show strong mixing in XXB. The maximum velocity of the upstream inflow and the intrusion flow from TGR reached 0.12 and 0.06 m·s$^{-1}$, respectively. The horizontal water exchange shows that the intrusion flow from TGR is transported to the upstream of the Xiangxi River, while the upstream inflow is transported to TGR.

In December, the water level of TGR slightly decreased from 170 m to 168 m. The upstream discharge was only 6 m$^3$·s$^{-1}$, and the water temperature was reduced to 13.4°C (3.5°C lower than that of TGR). The intrusion flow from TGR entered XXB in the lower and middle layer, whereas the upstream inflow moved along the river bed, and its velocity was reduced to zero at a distance of 10 km from the estuary (Figure 6(c)). It suggests that the upstream inflow is prevented from reaching to TGR, resulting in the nutrients enrichment in the river bed of XXB.

*3.3. The Static Stability.* The static stability can be generally utilized to evaluate the strength of density stratification:

$$E = -\frac{1}{\overline{\rho}}\frac{d\overline{\rho}}{dz}, \tag{2}$$

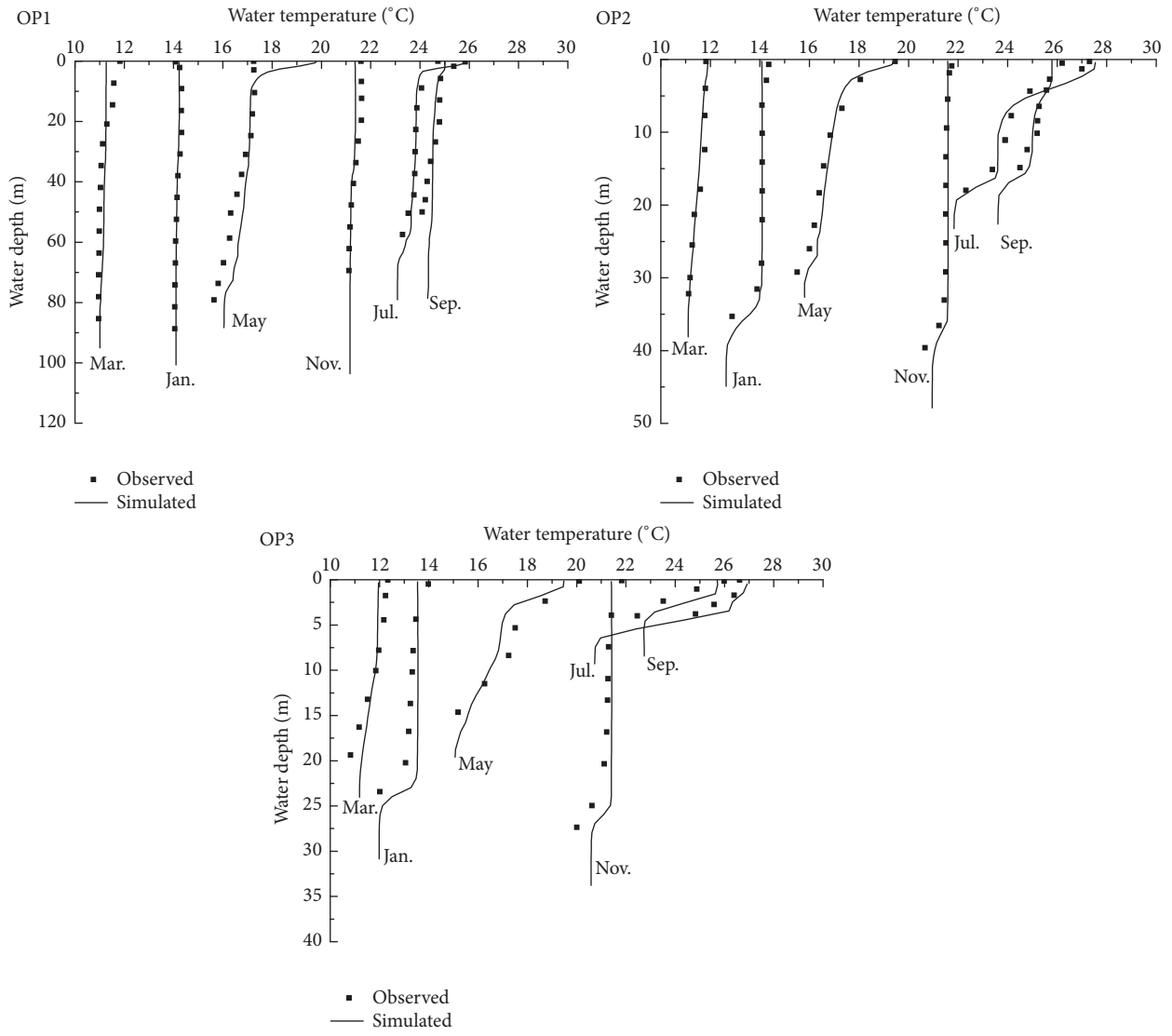


Figure 4: Observed and simulated vertical water temperature distribution of the 3 observation points in XXB (locations of the observation points are shown in "Figure 1").

where $E$ is static stability ($m^{-1}$), $z$ is water depth (m), and $\overline{\rho}$ is water density at depth $z$ ($kg \cdot m^{-3}$).

According to Lawrence et al. [21], water temperature stratification can be negligible when the water temperature gradient is less than $0.2^{\circ}C \cdot m^{-1}$. Therefore, the static stability in the condition that the water temperature gradient is $0.2^{\circ}C \cdot m^{-1}$ can be a critical value to judge stratification stability of XXB. The relationship between critical static stability and water temperature (from 10°C and 30°C) when the water temperature gradient is fixed at $0.2^{\circ}C \cdot m^{-1}$ (Figure 7) shows that the critical static stability increases with higher water temperature. In February, August, and December, the average water temperature of XXB was about 12, 26, and 16°C, respectively. Thus, the critical static stability in the 3 typical months was about $2.258 \times 10^{-5}$, $5.312 \times 10^{-5}$, and $3.338 \times 10^{-5}$ $m^{-1}$, respectively.

The vertical variation of the static stability at OP2 in the 3 typical months is shown in "Figure 8". The maximum value of the static stability in February was only $1.0 \times 10^{-5}$ $m^{-1}$ at a depth of 32 m, less than the critical value of this month, indicating that the water temperature was almost uniformly distributed. Water temperature stratification in February was negligible, which was consistent with the results of water temperature and flow velocity distribution. In August, 2 peak values of static stability can be observed along the vertical direction, consistent with the simulated water temperature distribution. The greatest static stability reached $3.0 \times 10^{-4}$ $m^{-1}$ and the second greatest was $0.9 \times 10^{-4}$ $m^{-1}$, both greater than the critical value of this month. Two stable thermoclines existed at a depth of 1 and 20 m, respectively, which restricted water and materials exchange effectively in the vertical direction. In December, the highest static stability

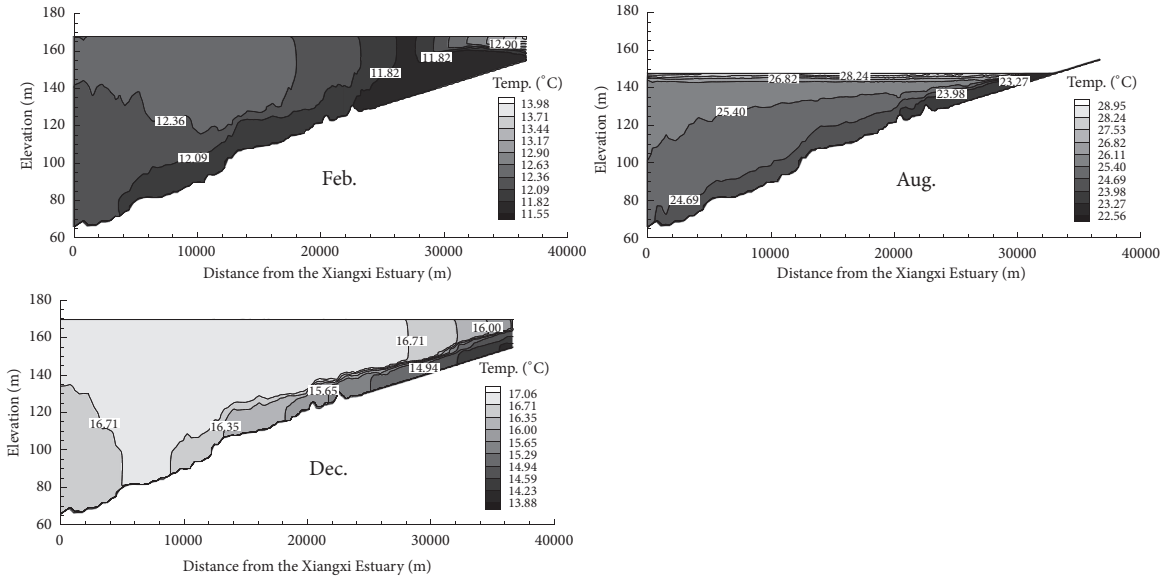


FIGURE 5: Thalweg water temperature profiles of the 3 typical months in XXB.

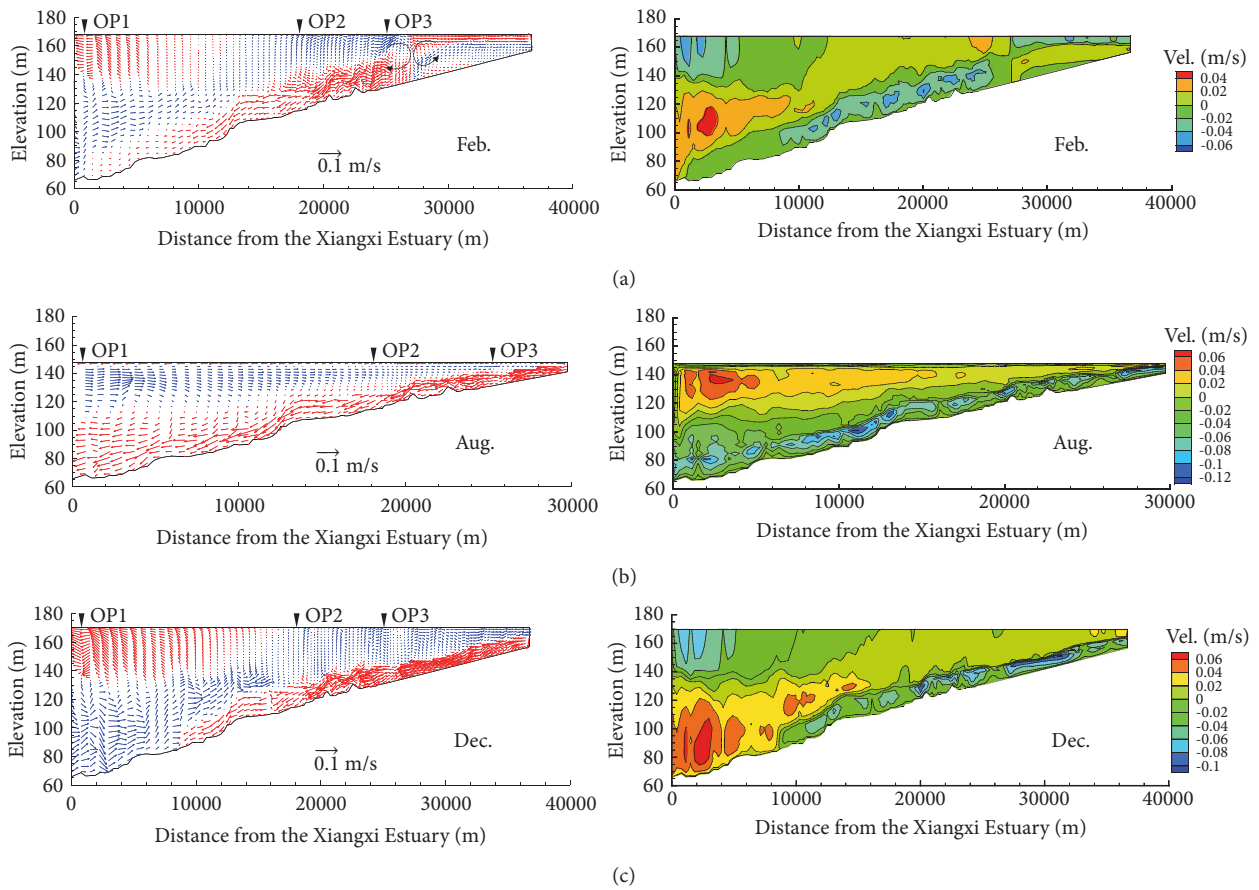


FIGURE 6: Thalweg profiles of velocity vectors (vectors are thinned in the vertical direction) and magnitude contours of the 3 typical months in XXB: (a) February represented the uniform distributed period; (b) August represented the strong stratification period; (c) December represented the bottom stratification period.

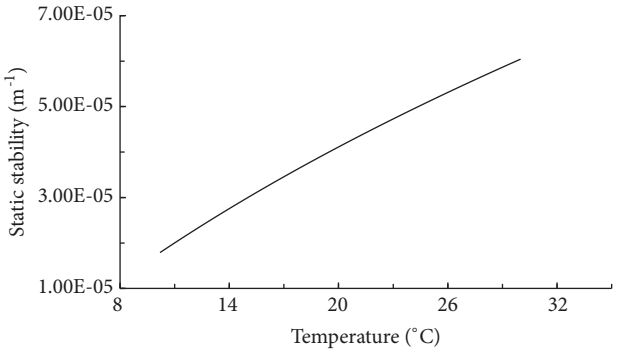


Figure 7: Relationship between the critical static stability and water temperature when the water temperature gradient is 0.2°C·m$^{-1}$.

was $0.9 \times 10^{-4}$ m$^{-1}$ at a depth of 38 m, larger than the critical value, providing a stable thermocline. The analysis of the static stability combined with the velocity vectors in December (Figure 6(c)) indicates that the thermocline near the river bed can prevent water exchange between upstream inflow and TGR.

*3.4. The Mixing Depth.* The mixing depth ($Z_{mix}$), defined as the depth where the vertical water temperature gradient is less than or equal to 0.2°C·m$^{-1}$ [21], is a critical parameter to evaluate the probability of spring algal blooms in XXB [5].

The annual variation of $Z_{mix}$ at the 3 observation points (Figure 9) shows that $Z_{mix}$ is deep in winter but is close to the water surface in summer. In spring, $Z_{mix}$ changed from lower layer to upper layer. $Z_{mix}$ of OP1 started to decrease after mid-April and stabilized at the beginning of May. However, $Z_{mix}$ of OP2 and OP3 both started to decrease at the beginning of March and also stabilized at the beginning of May. Contrary to that in spring, $Z_{mix}$ of all the 3 observation points began to increase in autumn.

Oliver et al. [22] suggested that the cumulative algal amount can be less than the lost amount when the value of $Z_{eup}/Z_{mix}$ ($Z_{eup}$ is euphotic depth) is less than 0.35 in spring. Reynolds et al. [23] considered that $Z_{eup}/Z_{mix} = 1$ is the most suitable condition for spring algal blooms. $Z_{eup}$, generally related to water turbidity, is less than 10 m year-round in XXB [24]. In spring, $Z_{mix}$ changed from deep region to near the surface and, as a result, $Z_{eup}/Z_{mix}$ can reach the most favorable condition for spring algal blooms. For the 3 observation points, the duration time of $Z_{mix}$ decrease at OP2 and OP3 was longer than that at OP1 (Figure 9), indicating that the spring algal blooms tended to occur in the upper and middle reach of XXB, which was consistent with the field observation conducted by Liu et al. [5].

*3.5. Cause of Spring Algal Blooms.* In general, sufficient nitrogen and phosphorus nutrients are the material basis for algae growth, and seasonal fluctuation of water temperature and sunlight condition are the main environmental conditions for algal blooms [25].

In-site monitoring has been applied to analyze the spatial and temporal distribution of nutrients in XXB [26–31]. From the space, the concentration of nitrogen nutrient fluctuated in XXB with higher concentration in the midstream, and the phosphorus nutrient gradually increased from the Xiangxi estuary to the upstream. From the time, the concentration of nitrogen nutrient decreased in spring, fluctuated in summer, decreased in autumn, and increased in winter. The phosphorus nutrient increased in spring, decreased in summer, fluctuated in autumn, and increased in winter.

Constant ion tracer technique and isotope tracer technique have been adopted to estimate the nutrient sources in XXB [29, 32–34]. Based on the law of mass conservation, the contribution rates of total nitrogen and total phosphorus in XXB from TGR were 94.83% and 86.13%, respectively. For the upper and middle reach of XXB where spring algal blooms are most prone to occur [35, 36], the upstream inflow dominated the supply of nutrients, and its contribution rates of total nitrogen and total phosphorus were 65.93% and 87.11%, respectively.

The general process of spring algal blooms in XXB can be inferred based on the analysis of hydrodynamic characteristics and mixing depth variation combined with monitoring results. In December and January, the upstream inflow transported nutrients and pollutants concentrated in the river bed among the upper and middle reach of XXB (consistent with the nutrients distribution and sources), which provided the material basis for spring algal blooms [37]. In February and March, the water temperature in XXB was almost uniformly distributed, and the strong water exchange in the vertical direction can transport the nutrients and pollutants in the river bed to the water surface. With increasing air temperature in spring, the water temperature and solar radiation would become favorable for algal growth (shown as the value of $Z_{eup}/Z_{mix}$); then algal blooms occurred. This process completely explained the cause of spring algal blooms in XXB.

*3.6. Measures to Alleviate Spring Algal Blooms.* Basically, forcing the concentration of nutrients lower than the critical concentration of the dominant algae proliferation by controlling nutrient sources is the most important measure to alleviate spring algal blooms in XXB. According to the analysis of spring algal blooms formation process, the enriched nutrients in the upper and middle reach of XXB are mainly supplied by the upstream inflow of the Xiangxi River Basin in winter. The direct measure to reduce the upstream nutrients is to control the agricultural nonpoint sources and point pollution sources (urban domestic and industrial sewage) in the Xiangxi River Basin, which requires a long period of time and a large amount of capital investment [38].

Comparing before and after impoundment of TGR, the main difference of XXB is the significant change in hydrodynamic conditions. Before the impoundment of TGR, the nutrients in the Xiangxi River were frequently transported to the Yangtze River due to strong water exchange, and there were no algal blooms. After the impoundment of TGR, the hydrodynamic conditions have been changed greatly, and algal blooms are observed in spring. This is because the specific hydrodynamic conditions cause the redistribution of nutrients in XXB, which provides the material basis

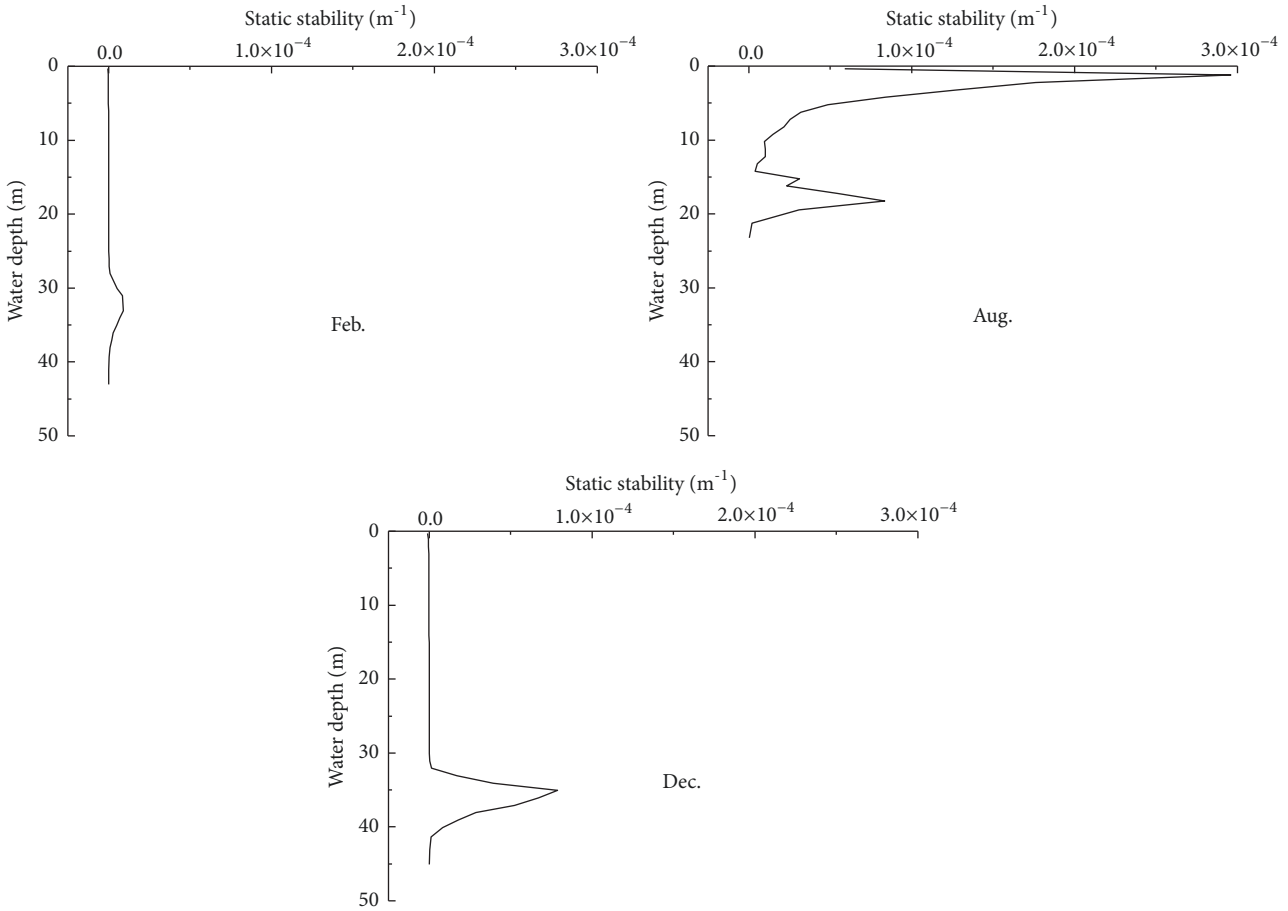


Figure 8: Vertical variation of the static stability at OP2 in the 3 typical months.

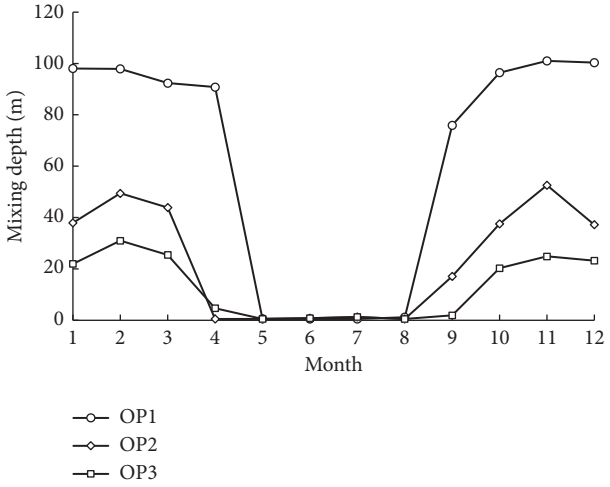


Figure 9: Annual variation of the mixing depth at the 3 observation points.

for spring algal blooms. Therefore, the reasonable measure to alleviate spring algal blooms is considered to improve the upstream hydrodynamic conditions and enhance the nutrients transport from XXB to TGR in winter.

The measure to improve the upstream hydrodynamic conditions can be realized through the operation of the hydraulic projects in the upstream of Xiangxi River Basin [39]. Considering there are more than 40 hydraulic projects in the Xiangxi River Basin which control the discharge flow, the ecological operation of the hydraulic projects needs further studies in the future research.

## 4. Conclusions

A 3D hydrodynamic and water temperature coupled model with the z-coordinate in the vertical direction was established to study the hydrodynamics, water temperature characteristics, and spring algal blooms in XXB, a typical tributary bay of TGR. The main conclusions are as follows.

(a) There are three types of water temperature distribution in XXB: the uniform distribution (from February to March), the strong stratification (from April to September), and the bottom stratification (from October to January).

(b) The upstream inflow is confined in XXB in either the no-stratification or bottom stratification period. However, during the strong stratification period, the upstream inflow generally flows into TGR along the river bed.

(c) The enriched nutrients in the upper and middle reach of XXB in winter offer the material basis for spring

algal blooms. Water temperature stratification that blocks nutrients transport in spring provides a suitable environment condition for algae growth, resulting in a possible reason for spring algal blooms in XXB.

(d) Improving the upstream hydrodynamic conditions and enhancing the nutrients transport from XXB to TGR in winter should be an effective measure to alleviate spring algal blooms in XXB.

## Data Availability

The data used to support the findings of this study are included within the article.

## Conflicts of Interest

The authors declare that there are no conflicts of interest regarding the publication of this paper.

## Acknowledgments

This work was financially supported by National Key R&D Program of China (2016YFC0401703, 2016YFC0401503), the National Natural Science Foundation of China (Grant nos. 51879086, 51479058, and 51609068), and the 111 Project (Grant no. B17015).

## References

[1] D. M. Anderson, P. M. Glibert, and J. M. Burkholder, "Harmful algal blooms and eutrophication: nutrient sources, composition, and consequences," *Estuaries and Coasts*, vol. 25, no. 4, pp. 704–726, 2002.

[2] Q. H. Cai and Z. Y. Hu, "Studies on eutrophication problem and control strategy in the three gorges reservoir," *Acta Hydrobiologica Sinica*, vol. 30, no. 01, pp. 7–11, 2006 (Chinese).

[3] Y. Xu, Q. Cai, L. Ye, S. Zhou, and X. Han, "Spring diatom blooming phases in a representative eutrophic bay of the three-gorges reservoir, China," *Journal of Freshwater Ecology*, vol. 24, no. 2, pp. 191–198, 2009.

[4] T. G. Zheng, J. Q. Mao, H. C. Dai, and D. F. Liu, "Impacts of water release operations on algal blooms in a tributary bay of three gorges reservoir," *Science China (Technological Sciences)*, vol. 54, no. 6, pp. 1588–1598, 2011.

[5] L. Liu, D. Liu, D. M. Johnson, Z. Yi, and Y. Huang, "Effects of vertical mixing on phytoplankton blooms in Xiangxi Bay of Three Gorges Reservoir: Implications for management," *Water Research*, vol. 46, no. 7, pp. 2121–2130, 2012.

[6] Z. J. Yang, P. Xu, D. Liu, J. Ma, D. Ji, and Y. Cui, "Hydrodynamic mechanisms underlying periodic algal blooms in the tributary bay of a subtropical reservoir," *Ecological Engineering*, vol. 120, pp. 6–13, 2018.

[7] Z. J. Yang, D. Liu, D. Ji, S. Xiao, Y. Huang, and J. Ma, "An eco-environmental friendly operation: An effective method to mitigate the harmful blooms in the tributary bays of three gorges reservoir," *Science China Technological Sciences*, vol. 56, no. 6, pp. 1458–1470, 2013.

[8] J. J. Lian, Y. Yao, C. Ma, and Q. Guo, "Reservoir operation rules for controlling algal blooms in a tributary to the impoundment of three gorges dam," *Water*, vol. 6, no. 10, pp. 3200–3223, 2014.

[9] Y. Sha, Y. Wei, W. Li, J. Fan, and G. Cheng, "Artificial tide generation and its effects on the water environment in the backwater of Three Gorges Reservoir," *Journal of Hydrology*, vol. 528, pp. 230–237, 2015.

[10] J. Ma, D. Liu, S. A. Wells, H. Tang, D. Ji, and Z. Yang, "Modeling density currents in a typical tributary of the Three Gorges Reservoir, China," *Ecological Modelling*, vol. 296, pp. 113–125, 2015.

[11] Z.-Z. Yu and L.-L. Wang, "Factors influencing thermal structure in a tributary bay of Three Gorges Reservoir," *Journal of Hydrodynamics*, vol. 23, no. 4, pp. 407–415, 2011.

[12] J. Q. Mao, D. G. Jiang, and H. C. Dai, "Spatial-temporal hydrodynamic and algal bloom modelling analysis of a reservoir tributary embayment," *Journal of Hydro-environment Research*, vol. 9, no. 2, pp. 200–215, 2015.

[13] J. Leendertse, "Turbulence modelling of surface water flow and transport: part IVa," *Journal of Hydraulic Engineering*, vol. 114, no. 4, pp. 603–606, 1990.

[14] G. S. Stelling and J. A. T. M. Van Kester, "On the approximation of horizontal gradients in sigma co-ordinates for bathymetry with steep bottom slopes," *International Journal for Numerical Methods in Fluids*, vol. 18, no. 10, pp. 915–935, 1994.

[15] H. X. Fang and T. Du, *Fundamentals of Oceanic Internal Waves and Internal Waves in the China Seas*, China Ocean University Press, Qingdao, China, 2005.

[16] P. H. Stone, "A simplified radiative-dynamical model for the static stability of rotating atmospheres," *Journal of the Atmospheric Sciences*, vol. 29, no. 3, pp. 405–418, 1972.

[17] H. U. Sverdrup, "On conditions for the vernal blooming of phytoplankton," *ICES Journal of Marine Science*, vol. 18, no. 3, pp. 287–295, 1953.

[18] WL/Delft, "Hydraulics User Manual Delft3D-FLOW," Deltares, Delft, The Netherland, 2011.

[19] UNESCO, "Background papers and supporting data on the international equation of state 1980," Tech. Rep. 38, 1981.

[20] V. Ouellet, Y. Secretan, A. St-Hilaire, and J. Morin, "Daily averaged 2D water temperature model for the St. Lawrence river," *River Research and Applications*, vol. 30, no. 6, pp. 733–744, 2014.

[21] I. Lawrence, M. Bormans, and R. Oliver, "Physical and nutrient factors controlling algal succession and biomass in Burrinjuck Reservoir," *Land and Water Resources Australia*, pp. 119-120, 2000.

[22] R. Oliver L, B. Hart T, and J. Olley, "The darling river: algal growth and the cycling and sources of nutrients," *Open Access This Report Has Been Reproduce with the Publishers Permission*, 1999.

[23] C. S. Reynolds, "Succession and vertical distribution of phytoplankton in response to thermal stratification in a lowland mere, with special reference to nutrient availability," *Journal of Ecology*, vol. 64, no. 2, pp. 529–551, 1976.

[24] X. Yang, *Main Controlling Factors of Algal Bloom under Reverse Density Current in Xiangxi Bay of Three Gorges Reservoir*, China Three Gorges University, Yichang, Hubei, China, 2011.

[25] G. J. Zhou, X. M. Zhao, and Y. H. Bi, "Phytoplankton variation and its relationship with the environment in Xiangxi Bay in spring after damming of the three-gorges," *China Environmental Monitoring and Assessment*, vol. 176, no. 1-4, pp. 125–141, 2011.

[26] T. Fang, Y. C. Fu, and H. Ao, "The comparison of phosphorus and ni-trogen pollution status of the Xiangxi Bay before and after the impoundment of the Three Gorges reservoir," *Acta Hydrobiologica Sinica*, vol. 30, no. 01, pp. 26–30, 2006 (Chinese).

[27] H. Dai, T. Zheng, and D. Liu, "Effects of reservoir impounding on key ecological factors in the three gorges region," in *Proceedings of the International Conference on Ecological Informatics and Ecosystem Conservation, ISEIS 2010*, pp. 15–24, China, August 2010.

[28] Y. Zhang, D.-F. Liu, D.-B. Ji, Z.-J. Yang, and Y.-Y. Chen, "Effects of intrusions from Three Gorges Reservoir on nutrient supply to Xiangxi Bay," *Environmental Science*, vol. 33, no. 8, pp. 2621–2627, 2012 (Chinese).

[29] F. D. Liu, L. Y. Huang, and B. D. Ji, *Tributary Algal Blooms and Ecological Operation of Three Gorges Reservoir*, China Water Conservancy and Hydropower Press, Beijing, China, 2013.

[30] A. Holbach, S. Norra, L. Wang et al., "Three Gorges Reservoir: Density pump amplification of pollutant transport into tributaries," *Environmental Science & Technology*, vol. 48, no. 14, pp. 7798–7806, 2014.

[31] Y. L. Huang, P. Zhang, D. F. Liu, Z. Yang, and D. Ji, "Nutrient spatial pattern of the upstream, mainstream and tributaries of the Three Gorges Reservoir in China," *Environmental Modeling & Assessment*, vol. 186, no. 10, pp. 6833–6847, 2014.

[32] X. B. Ran, Z. G. Yu, Q. Z. Yao, H. Chen, and T. Mi, "Major ion geochemistry and nutrient behaviour in the mixing zone of the Changjiang (Yangtze) River and its tributaries in the Three Gorges Reservoir," *Hydrological Processes*, vol. 24, no. 17, pp. 2481–2495, 2010.

[33] Y. Chen, D. Liu, Z. Yang et al., "The impacts of the stratified density currents on supply pattern of main nutrients in Xiangxi River," *Acta Scientiae Circumstantiae*, vol. 33, no. 3, pp. 762–770, 2013.

[34] L. Yang, D. Liu, Y. Huang, Z. Yang, D. Ji, and L. Song, "Isotope analysis of the nutrient supply in Xiangxi Bay of the Three Gorges Reservoir," *Ecological Engineering*, vol. 77, pp. 65–73, 2015.

[35] L. Ye, X. Q. Han, Y. Y. Xu, and Q. H. Cai, "Spatial analysis for spring bloom and nutrient limitation in Xiangxi bay of three Gorges Reservoir," *Environmental Modeling & Assessment*, vol. 127, no. 1-3, pp. 135–145, 2007.

[36] Z. J. Yang, *Modeling The Algae Bloom Based on The Vertical Migration of Phytoplankton in Xiangxi Bay and Its Control Methods by Scheduling The Three Gorges Reservoir's Operation*, China Three Gorges University, Yichang, Hubei, China, 2010.

[37] A. Holbach, Y. Bi, Y. Yuan, L. Wang, B. Zheng, and S. Norra, "Environmental water body characteristics in a major tributary backwater of the unique and strongly seasonal Three Gorges Reservoir, China," *Environmental Science: Processes & Impacts*, vol. 17, no. 9, pp. 1641–1653, 2015.

[38] B.-J. Fu, B.-F. Wu, Y.-H. Lü et al., "Three Gorges Project: efforts and challenges for the environment," *Progress in Physical Geography*, vol. 34, no. 6, pp. 741–754, 2010.

[39] L. Wang, C. H. Dai, and Q. H. Cai, "Numerical simulation of the ecological operation schedule in Xiangxi river," *Huazhong University of Science and Technology (Natural Science Edition)*, vol. 37, no. 4, pp. 111–114, 2009.